Biochimica et Biophysica Acta 1863 (2017) 188–199

Contents lists available at ScienceDirect

Biochimica et Biophysica Acta

journal homepage: www.elsevier.com/locate/bbadis

Leucine 208 in human histamine *N*-methyltransferase emerges as a hotspot for protein stability rationalizing the role of the L208P variant in intellectual disability

Chanakan Tongsook, Johannes Niederhauser, Elena Kronegger, Grit Straganz, Peter Macheroux *

Graz University of Technology, Institute of Biochemistry, Petersgasse 12/II, A-8010 Graz, Austria

ARTICLE INFO

Article history:
Received 13 June 2016
Received in revised form 20 September 2016
Accepted 11 October 2016
Available online 18 October 2016

Keywords:
Isothermal titration calorimetry
Molecular dynamics simulations
Neurotransmitter
Protein stability
S-adenosylmethionine

ABSTRACT

The degradation of histamine catalyzed by the SAM-dependent histamine *N*-methyltransferase (HNMT) is critically important for the maintenance of neurological processes. Recently, two mutations in the encoding human gene were reported to give rise to dysfunctional protein variants (G60D and L208P) leading to intellectual disability. In the present study, we have expressed eight L208 variants with either apolar (L208F and L208V), polar (L208N and L208T) or charged (L208D, L208H, L208K and L208R) amino acids to define the impact of side chain variations on protein structure and function. We found that the variants L208N, L208T, L208D and L208H were severely compromised in their stability. The other four variants were obtained in lower amounts in the order wild-type HNMT > L208F = L208 V > L208 K = L208R. Biochemical characterization of the two variants L208F and L208V exhibited similar Michaelis-Menten parameters for SAM and histamine while the enzymatic activity was reduced to 21% and 48%, respectively. A substantial loss of enzymatic activity and binding affinity for histamine was seen for the L208K and L208R variants. Similarly the thermal stability for the latter variants was reduced by 8 and 13 °C, respectively. These findings demonstrate that position 208 is extremely sensitive to side chain variations and even conservative replacements affect enzymatic function. Molecular dynamics simulations showed that amino acid replacements in position 208 perturb the helical character and disrupt interactions with the adjacent β-strand, which is involved in the binding and correct positioning of histamine. This finding rationalizes the gradual loss of enzymatic activity observed in the L208 variants.

1. Introduction

Histamine, [2-(1H-imidazol-4-yl)ethanamine], is a biogenic amine that plays important roles in several physiological and pathological processes including the regulation of inflammatory and immune responses, gastric acid secretion and bronchial asthma [1–4]. Histamine also functions as a neurotransmitter in the central nervous system (CNS) where it contributes to the regulation of many processes such as the sleep/wake cycle, the circadian rhythm, thermoregulation, stress and fluid homeostasis [5–7]. Furthermore, histamine acts as a key neuromodulator in the developing nervous system. In the embryonic state of the developing rat brain the maximum level of histamine concentration coincides with the period where neuronal differentiation takes place in several brain regions [8–10]. Histidine decarboxylase, a pyridoxal 5′-phosphate (PLP)-dependent enzyme, catalyzes the decarboxylation of the amino acid L-histidine to generate histamine, which is stored in granules in airway mast cells, basophils and enterochromaffine cells [5,11]. Release of histamine from cells is triggered upon the cross-linking surface-bound immunoglobulin E (IgE) by allergens [12]. The actions of released histamine are mediated through the four histamine receptors (H1R—H4R), which belong to the rhodopsin-like family of G protein-coupled receptors [13–15]. H1R, H2R and H3R are expressed in abundance in the brain whereas H4R is expressed mainly in peripheral tissues (*e.g.* the gut and connective tissue) [14,16]. Released histamine is then rapidly inactivated and disappears from the bloodstream within minutes [5].

In mammals, the action of histamine is terminated by either one of two mechanisms that involve the methylation of the imidazole ring or the oxidative deamination of the primary amino group. The former reaction is catalyzed by histamine *N*-methyltransferase (HNMT; EC 2.1.1.8) and the latter reaction by diamine oxidase (DAO; EC 1.4.3.22) [17]. Products generated from these two enzymatic reactions are virtually inactive at histamine receptors and are further converted for transport and secretion [18,19]. HNMT is the primary metabolizing enzyme for released histamine in bronchial epithelial cells, endothelial cells of human airways and the human stomach [20,21]. In addition,

Abbreviations: CNS, central nervous system; DAO, diamine oxidase; HNMT, histamine *N*-methyltransferase; MTase, methyltransferase; SAM, *S*-adenosylmethionine; SAH, *S*-adenosylhomocysteine.

* Corresponding author.
E-mail address: peter.macheroux@tugraz.at (P. Macheroux).

http://dx.doi.org/10.1016/j.bbadis.2016.10.005

HNMT is also the only enzyme responsible for the termination of histamine action in the mammalian brain, since the other histamine-metabolizing enzyme, DAO, is not expressed in the CNS [5,22]. DAO, an enzyme of the class of copper-containing amine oxidases, is the main histamine-degrading enzyme in peripheral tissue including termination of exogenous histamine from ingestion (food and alcohol) [14].

HNMT inactivates histamine by transferring a methyl group from *S*-adenosylmethionine (SAM), to the $N_{\varepsilon 2}$ atom of the imidazole ring, generating *N*-methylhistamine and *S*-adenosylhomocysteine (SAH) [23,24]. Enzyme activity and mRNA transcription were found in most human tissues with the highest levels in kidney and liver as well as substantial levels observed in spleen, prostate, ovary, intestine and the spinal cord and lower levels in the heart, brain, placenta, lung, stomach and thyroid gland [18,25]. The *HNMT* gene is approximately 34 kb in length, located on chromosome 2q22.1, and consists of 6 exons [26–28]. Production and characterization of human HNMT showed that cytoplasmic HNMT has 292 amino acid residues with a total molecular mass of 33 kDa [18]. Several three-dimensional structures of HNMT with bound SAH and histamine as well as various HNMT inhibitors revealed that HNMT is a monomeric protein and consists of two domains. The large domain adopts a canonical methyltransferase (MTase) fold with a SAM binding pocket, whereas the small domain contributes part of the histamine binding pocket and may be involved in protein-protein interactions. The bound histamine is buried in a hydrophobic pocket (surrounded by 14 aromatic amino acid residues) at the interface of the two domains. Amino acid residues that interact with SAH and histamine are highly conserved in vertebrates [29,30].

Since disturbances of histamine metabolism have been related to several diseases, *i.e.* asthma, bronchial hyper-responsiveness (BHR), neurological disorders, the lack of transcription or decrease in HNMT activity have been proposed as a causative factor for these diseases. A common single nucleotide polymorphism (SNP), c.314C>T transition (prevalence 0.1), resulting in the replacement of T105 for isoleucine was associated with decreased enzyme activity, immunoreactive protein, and thermal stability [25]. Steady-state kinetics revealed that the apparent Michaelis constants (K_M) increased 1.8 and 1.3 fold for SAM and histamine, respectively, and showed a reduction of the specific activity of about 16% [29]. Moreover, from multiple molecular dynamic (MD) simulations, isoleucine 105 apparently more strongly interacts with neighboring residues leading to a disordering of several key residues responsible for SAM binding and lower hydrophobicity of the substrate-binding site [31]. Thus, the polymorphic T105I variant has been proposed to associate with several diseases including asthma, allergic rhinitis, essential tremor and Parkinson's disease [32–35].

Intellectual disability (ID) is a common neurodevelopmental disorder characterized by an intelligence quotient of 70 or below with deficits in adaptive, daily living skills and intellectual functioning manifesting before the age of 18 [36]. With a prevalence of about 1% of children worldwide, ID is one of the major socioeconomic problems [37]. Recently, two other homozygous missense mutations in the *HNMT* gene were identified in patients affected with nonsyndromic autosomal recessive intellectual disability (ND-ARID) from two unrelated consanguineous families of Turkish and Kurdish ancestry [38]. The first mutation (*HNMT* c.179G>A) from the Turkish family resulting in a change of G60 to aspartate (G60D) occurs in the conserved MTase region I, which is part of the SAM-binding pocket. This amino acid exchange impedes binding of SAM as shown in our previous work [38]. As a consequence, the G60D variant does not show any activity in the methylation of histamine and thus the pathway of histamine inactivation is blocked. The other mutation (*HNMT* c.632T>C) found in the Kurdish family results in the replacement of L208 for proline (L208P). This invariant residue is located in helix E of the MTase domain and forms several hydrophobic interactions with neighboring residues. Interestingly, L208 is located in a considerable distance from the active site (*ca.* 18 Å from the substrate binding pocket) (Fig. 1, panels A-C) suggesting that the adverse effect of the amino acid replacement is caused by perturbations of the protein structure leading to compromised enzyme function. In fact, previous attempts to express the L208P variant were not successful [38]. In order to better understand the role and importance of L208 in maintaining protein structure, stability and enzyme function we have engaged in a more detailed analysis by generating a series of variants with either apolar (L208V and L208F), polar (L208T and L208N) or charged (L208R, L208K, L208H, and L208D) amino acid replacements. In the present study we report the biochemical properties of the variants that were successfully expressed. In addition, we have investigated the role of L208 and the impact of variations in this position by a set of molecular dynamic simulations. Taken together these methods have provided detailed insights into the functional and structural role of L208 and provide a rationale for the disease causing effect of mutations affecting this amino acid position.

2. Materials and methods

2.1. Reagents

All chemicals and reagents were of the highest purity commercially available from Sigma-Aldrich, Merck, and Carl Roth GmbH & Co. KG. [Methyl-^{3}H]-SAM and Ultima Gold liquid scintillation cocktail were from PerkinElmer. Ni-Sepharose (prepacked HisTrap™ HP) and Superdex 200 prep grade (HiLoad 16/600 Superdex 200 pg) columns were from GE Healthcare (Little Chalfont, UK). HNMT (wild-type) and L208 variants were overexpressed in *Escherichia coli* and purified as previously described [38]. The concentrations of the following compounds were determined spectrophotometrically using the respective extinction coefficients: SAM and SAH, $\varepsilon_{260} = 15.4\ mM^{-1}\ cm^{-1}$ [39]; and HNMT (wild-type and L208 variants, based on amino acid sequence), $\varepsilon_{280} = 42.8\ mM^{-1}\ cm^{-1}$.

2.2. Site-directed mutagenesis

Site-directed mutagenesis at position L208 was performed using QuickChange® Site-Directed Mutagenesis Kit (Stratagene, La Jolla, *CA*, USA). The mutagenic forward primers and the reverse primers (Supplemental Table S1) were from VBC-Biotech Service GmbH (Vienna, Austria). The plasmid pET-21a harboring *HNMT* (wild-type) gene was used as the template for mutagenic PCR. PCR reactions (18 cycles of the standardized protocol) were performed using a PCR instrument with GeneAmp PCR system, Applied Biosystem® (Thermo Fisher Scientific, Waltham, MA, USA). The DNA sequences of all variant plasmids were analyzed using the forward primers 5′-TAATACGACTCACTATAGGG-3′ (T7-Promoter) and the reverse primer 5′-GCTAGTTATTGCTCAGCGG-3′ (T7-terminator) by LGC Genomics (Teddington, UK).

2.3. Protein production and purification of HNMT (wild-type) and L208 variants in Escherichia coli

Protein production and purification of HNMT (wild-type) and L208 variants (L208V, L208F, L208T, L208N, L208R, L208K, L208H, and L208D) with C-terminal His6 tag in *Escherichia coli* was performed: *E. coli* BL21 (DE3) was transformed with the plasmid pET-21a harboring *HNMT* (wild-type or mutated L208) genes. A colony of the transformants was inoculated in lysogen broth (LB) containing 100 μg/mL of ampicillin to prepare a preculture, which was aerobically incubated at 37 °C and 150 rpm for 16 h. The precultured cells (1% of cell inoculation) were transferred to 10 L of LB containing 100 μg/mL of ampicillin. Cells were grown at 37 °C and 150 rpm until the absorption at 600 nm of the cell culture reached ~1.0. Synthesis of the recombinant protein was induced by adding 0.1 mM of isopropyl β-D-thiogalactopyranoside (IPTG). The cell culture was further grown at 18 °C and 150 rpm for 16 h. Cells were harvested using centrifugation at 5000 *g* for 10 min. Cell paste was kept at −70 °C until used.

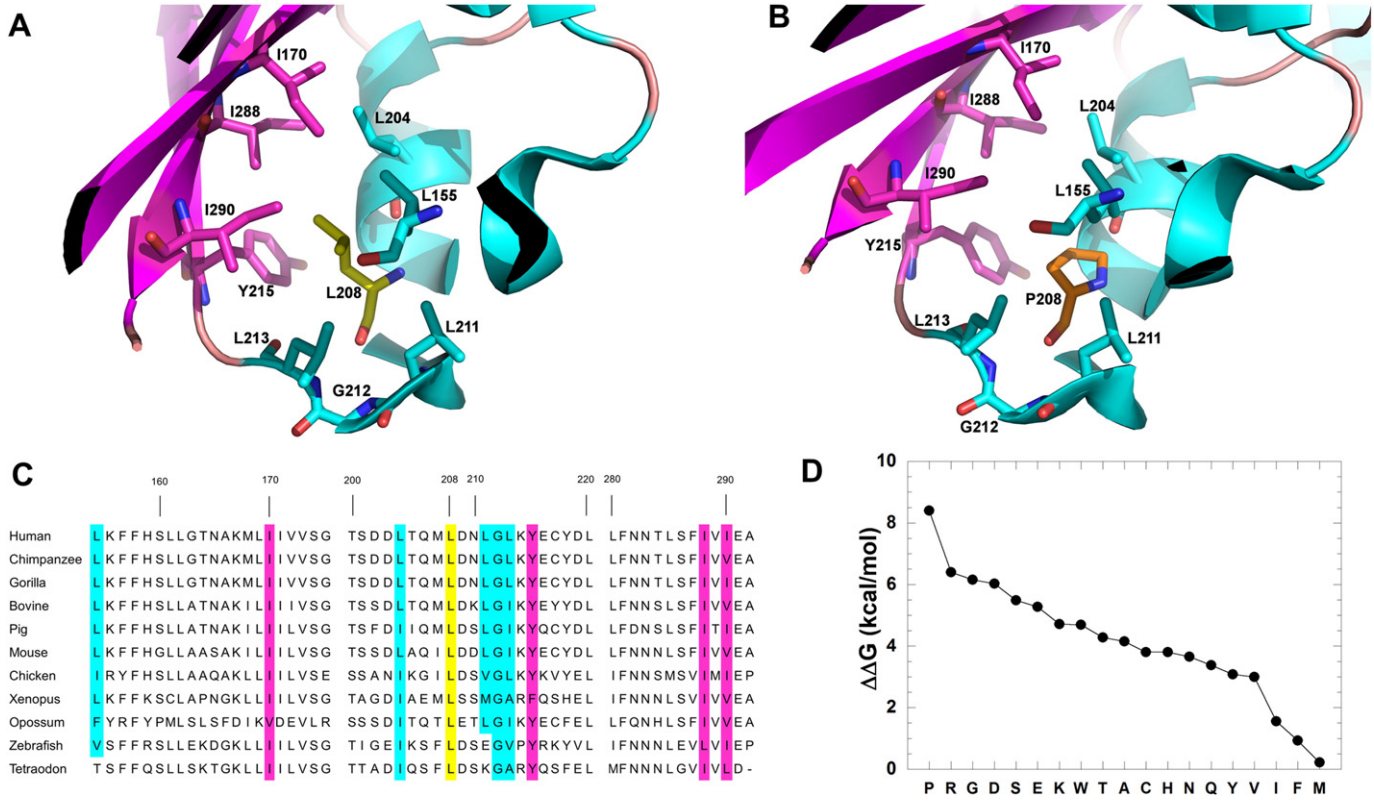

Fig. 1. Structure of HNMT with a focus on position 208, sequence alignment and protein stability analysis. Cartoon of HNMT variant structures depicting sections of the hydrophobic pockets around residue 208 for L208 (wild-type) in yellow (A) and L208P in orange (B) with surrounding apolar residues: I170, Y215, I288, and I290 in purple and L155, L204, L211, G212, L213 in light blue. (C) Protein sequence alignment of HNMT homologs using Clustal Omega 1.2.1 (www.clustal.org/omega) at the hydrophobic pocket surrounding residue L208. The L208 is highlighted in yellow. Residues I170, Y215, I288, and I290 were highlighted in purple and residues L155, L204, L211, G212, L213 in light blue. All HNMT sequences used for the alignment were obtained from NCBI Reference Sequence Database: human (NP_008826.1), chimpanzee (XP_001156140.1), gorilla (XP_004032652.1), bovine (NP_001030511.1), pig (NP_001166431.1), mouse (NP_536710.1), chicken (NP_001264802.1), xenopus (NP_001080614.1), opossum (UniProtKB browser_F6X9A6), zebrafish (NP_001003636.1), and tetraodon (Q4SB6.1). (D) Effect of amino acid substitutions at position 208 on protein stability as calculated by SNPeffect 4.0 (FoldX) expressed as the difference to wild-type protein (ΔΔG in kcal/mol).

To purify HNMT (wild-type) and L208 variants, frozen cell paste of the wild-type or L208 variants was thawed and resuspended in lysis buffer using 2.5 mL of buffer/g of cell paste. This buffer contained 50 mM Tris-HCl pH 8.0, 100 mM NaCl, 10 mM imidazole, 1 mM DTT, 100 μM PMSF and supplemented with protease inhibitors (Roche complete EDTA-free protease inhibitor cocktail, Roche). Cells were disrupted using ultrasonication with 50% amplitude for 15 min. Cell debris and unbroken cells were removed from the cell lysate to gain the clear crude extract using centrifugation at 40,000 *g* and 4 °C for 1 h. The clear crude extract was filtrated (0.45 μm) and then applied onto a 5-mL Ni-Sepharose HisTrap™ HP column (GE-Healthcare, Little Chalfont, UK) previously equilibrated with 50 mM Tris-HCl pH 8.0, 300 mM NaCl and 10 mM imidazole. The column was washed with 50 mM Tris-HCl buffer pH 8.0 containing 300 mM NaCl and 20 mM imidazole. HNMT was eluted using 50 mM Tris-HCl buffer, pH 8.0 containing 300 mM NaCl and 300 mM imidazole. Eluted fractions containing HNMT were pooled, and then concentrated using a Centricon YM10 with 10 kDa cut-off. The concentrated protein fraction was loaded onto a Superdex 200 prep grade column (HiLoad 16/600 Superdex 200 pg, GE-Healthcare, Little Chalfont, UK) previously equilibrated with 50 mM Tris-HCl pH 8.0 containing 100 mM NaCl. HNMT fractions were pooled and then concentrated as described before. The purified HNMT was flash frozen in liquid nitrogen and stored at −70 °C until used. To check protein purity and subunit molecular mass of HNMT, aliquots of the protein fractions were analyzed using 12.5% SDS-PAGE and staining with Coomassie Brilliant Blue R250. Catalytic activity for histamine *N*-methyltransferase of the protein fractions was determined using a radioactive methylation assay as described below.

2.4. Western blotting

Protein samples for western blot analysis were separated using 12.5% SDS-PAGE and then electrically transferred to a nitrocellulose membrane by applying electricity (150 mA) from a power supply for 1 h. The membrane was blocked for 1 h using 13% milk powder in TBS buffer (50 mM Tris-HCl buffer pH 8.0 and 150 mM NaCl) containing 0.1% tween-20. The membrane was incubated with the primary rabbit His-Tag antibody (1:1000 dilution, Cell Signaling Technology®, Danvers, MA, USA) for 16 h, and then incubated with the secondary antibody *anti*-rabbit IgG, horseradish peroxidase-linked antibody (1:5000 dilution, Cell Signaling Technology®, Danvers, MA, USA) for 1 h. To detect chemiluminescent signal of antibody-bound His6 tagged HNMT, the immunoblots were developed using enhanced chemiluminescent western blotting substrate solution (Pierce-Thermo Fisher Scientific, Waltham, MA, USA).

2.5. Determination of melting temperature of HNMT (wild-type) and L208 variants

To investigate the thermal stability of HNMT (wild-type) and L208 variants in the absence and presence of substrates, SAM and histamine, the melting temperature was determined by a fluorescence-based thermal shift assay, using SYPRO Orange (Sigma-Aldrich, St. Louis, MO, USA). Experiments were performed in a CFX Connect™ real-time PCR detection system (Bio-Rad, Hercules, *CA*, USA) with a 96-well plate in FRET scan mode. To prepare protein samples for the measurement, 5 μL of 1 mg/mL HNMT (wild-type or L208 variants) were mixed with 5 μL of SYPRO Orange solution (200-fold dilution) and 15 μL of a buffer containing 50 mM Tris-HCl pH 8.0 and 100 mM NaCl to a final volume of

25 μL in a 96-well plate. The protein samples in the presence of substrate (SAM or histamine) were prepared similarly as described above but either SAM or histamine was added to a final concentration of 2 mM. A temperature gradient from 20 °C to 95 °C was set to monitor thermal unfolding of the protein, measuring fluorescence emission at 0.5 °C increments with a 60 s hold for signal stabilization. The melting temperature of the protein in the absence and presence of substrates was obtained from the peak of the derivatives of the experimental data.

2.6. Determination of dissociation constants (K_d) of HNMT (wild-type) and L208 variants

All of the experiments to investigate dissociation constants (K_d) for SAM, SAH, and histamine to HNMT (wild-type) and L208 variants and for histamine to the binary complex of HNMT:SAH were performed using a VP-ITC system (MicroCal, Northampton, MA, USA) in 50 mM Tris-HCl buffer pH 8.0 containing 100 mM NaCl at 25 °C. All solutions were degassed before measurements. The HNMT (wild-type) solution (30 μM) was injected with SAM (0.42 mM), SAH (0.38 mM), or histamine (4 mM) (20 injections, 15 μL/injection, duration time 29.9 s, spacing time 250 s). Titration experiments for SAM, SAH and histamine binding to the L208V and L208F variants were set to 20 injections of 15 μL of 0.7 mM SAM, 0.55 mM SAH, or 4 mM histamine, respectively, (duration time 29.9 s, spacing time 250 s) into the cell containing 30 μM HNMT (L208V and L208F). To determine the K_d of L208R and L208K variants for SAM, SAH, and histamine, 20 μM of the HNMT proteins were titrated with SAM (1 mM), SAH (0.8 mM), or 4 mM histamine (20 injections, 15 μL/injection, duration time 29.9 s, spacing time 250 s). For the determination of the dissociation constants for histamine to the binary HNMT (wild-type, L208V, and L208K):SAH complex (20 μM HNMT:120–250 μM SAH), histamine (0.58 mM for HNMT (wild-type) and 0.50 mM for the L208 variants) was titrated into the complex solution (20 injections, 15 μL/injection, duration time 29.9 s, spacing time 250 s). The K_d values of HNMT (wild-type) and L208 variants for SAM, SAH, histamine, and histamine in the presence of SAH were obtained fitting the data to a single-binding-site model with Origin version 7.0 (MicroCal, Northampton, MA, USA) for ITC data analysis.

2.7. Determination of catalytic activity of HNMT (wild-type) and L208 variants

To measure catalytic activity of HNMT (wild-type) and L208 variants; L208V, L208F, L208R, and L208 K, radioactive methylation assays were performed at 25 °C. [Methyl-^{3}H]-SAM was utilized and the methylation reaction was monitored by formation of the product, [methyl-^{3}H]-histamine [29,40,41]. The assay reaction in a 1.5 mL Eppendorf tube contained 20 nM HNMT (wild-type or L208 variants), 40 μM unlabeled SAM, 40 μM histamine, 0.158 μCi [methyl-^{3}H]-SAM, 1 mM EDTA, and 0.025% bovine serum albumin in 125 mM bicine buffer pH 8.0 to make up a final volume of 100 μL. The reaction mixture was preincubated at 25 °C for 2 min prior to the addition of histamine to initiate the reaction. The termination of the reaction was conducted by adding 75 μL of 1 M sodium borate pH 11 after the reaction was incubated at 25 °C for 30 min. The product, [methyl-^{3}H]-histamine, was isolated from unincorporated [methyl-^{3}H]-SAM in the reaction by organic extraction by adding 1:1 toluene:isoamyl alcohol (1.25 mL). After vortexing and centrifugation at 21,100 *g* for 1 min, 1 mL of the organic phase was transferred to a 1.5 mL Eppendorf tube and then mixed with 250 μL of 0.5 M HCl. The tube was again vortexed and centrifuged to facilitate phase separation. 200 μL of the aqueous phase were transferred to a scintillation vial containing 10 mL of Ultima Gold liquid scintillation cocktail (PerkinElmer, Waltham, MA, USA). After mixing, the vial was quantified by scintillation spectrometry. To determine the variant's and wild-type enzymes' kinetic parameters, K_M and k_{cat}, for SAM, histamine was fixed at saturating concentration of 40 μM and the concentration of SAM was varied in the range of 5–80 μM. In order to obtain the respective kinetic parameters for histamine, the SAM concentration was kept constant at 40 μM and histamine concentration was varied in the range of 1–20 μM. Data analysis to obtain the kinetic parameters was performed by plotting the rate of [methyl-^{3}H]-histamine formation normalized by the HNMT concentration (v/e) *versus* the substrate concentration (SAM or histamine) and fitting the data points using Marquardt-Lavenberg algorithms in the KaleidaGraph program (Synergy Software, Reading, PA, USA). The data points shown in the plots represent the mean of two independent measurements.

2.8. Measurements of circular dichroism (CD) spectrometry

To determine the secondary structure of HNMT (wild-type) and L208 variants, circular dichroism (CD) spectrometry was performed using a Jasco J715 spectropolarimeter (JASCO Inc., Tokyo, Japan) equipped with thermostat cell compartments. The CD spectra of HNMT in the far UV region (260–185 nm) were recorded in quartz cells with path length 0.02 cm (Hellma, Forest Hills, NY, USA) with a scan speed of 100 nm/min at 25 °C, averaged over three scans and corrected by the blank signal. HNMT was prepared in 20 mM

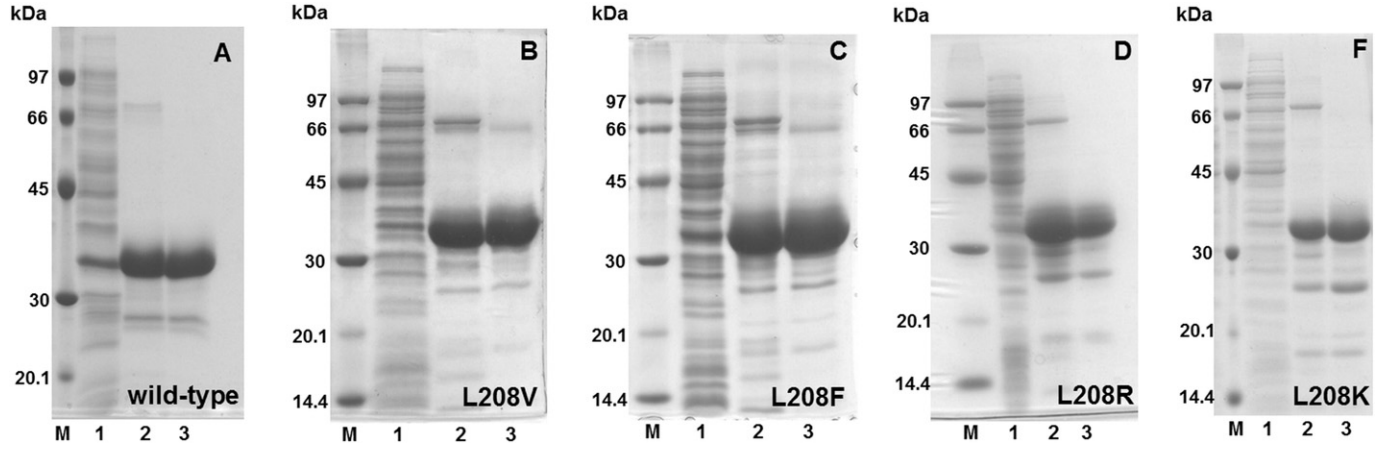

Fig. 2. Protein production and purification for HNMT (wild-type) and L208 variants. The recombinant HNMT (wild-type) and L208 variants were expressed in *E.coli* and purified using Ni-Sepharose affinity and Superdex 200 size-exclusion chromatography. SDS-PAGE (12.5%) analysis of HNMT (wild-type) (A) and L208 variants: L208V (B), L208F (C), L208R (D), and L208K (F) after each step of the protein purification. Each lane was loaded with either 20 (wild-type, L208R and L208K variants) or 25 μg (L208V and L208F variants). Lane M, low molecular mass protein marker; lane 1, crude extract; lane 2, the protein fraction after Ni-Sepharose chromatography; lane 3, the protein fraction after Superdex 200 size-exclusion chromatography.

Table 1
Protein purification table for HNMT (wild-type) and soluble L208 variants.

Step of protein purification	Wild-type		L208V		L208F		L208R		L208 K	
	total protein (mg)	% yield	total protein (mg)	% yield	total protein (mg)	% yield	total protein (mg)	% yield	total protein (mg)	% yield
Crude extract	1727	100	1305	100	1307	100	1243	100	3852	100
Ni-Sepharose	197	11	64	5	68	5	42	3	43	1
Superdex 200	111 (6)[a]	6	37 (2)[a]	3	41 (2)[a]	3	7 (0.2)[a]	0.5	16 (0.4)[a]	0.4

Starting cell paste for protein purification for HNMT (wild-type), L208 V, L208F, L208R, and L208K variants was 20, 19, 19, 30, and 45 g respectively.
[a] Amount of protein in mg per g of cell paste (mg/g) is shown in parentheses.

Tris-acetate buffer pH 8.0 to give a final concentration in the range of 0.6–1 mg/mL. The secondary structure content of HNMT (wild-type) and L208 variants was analyzed using the Spectra Manager program (JASCO Inc., Tokyo, Japan) and the web tool DichroWeb [42,43].

2.9. MALDI-TOF mass spectrometry

Protein extraction from polyacrylamide gels and MALDI-TOF mass spectrometric measurements for HNMT (wild-type) and L208 variants

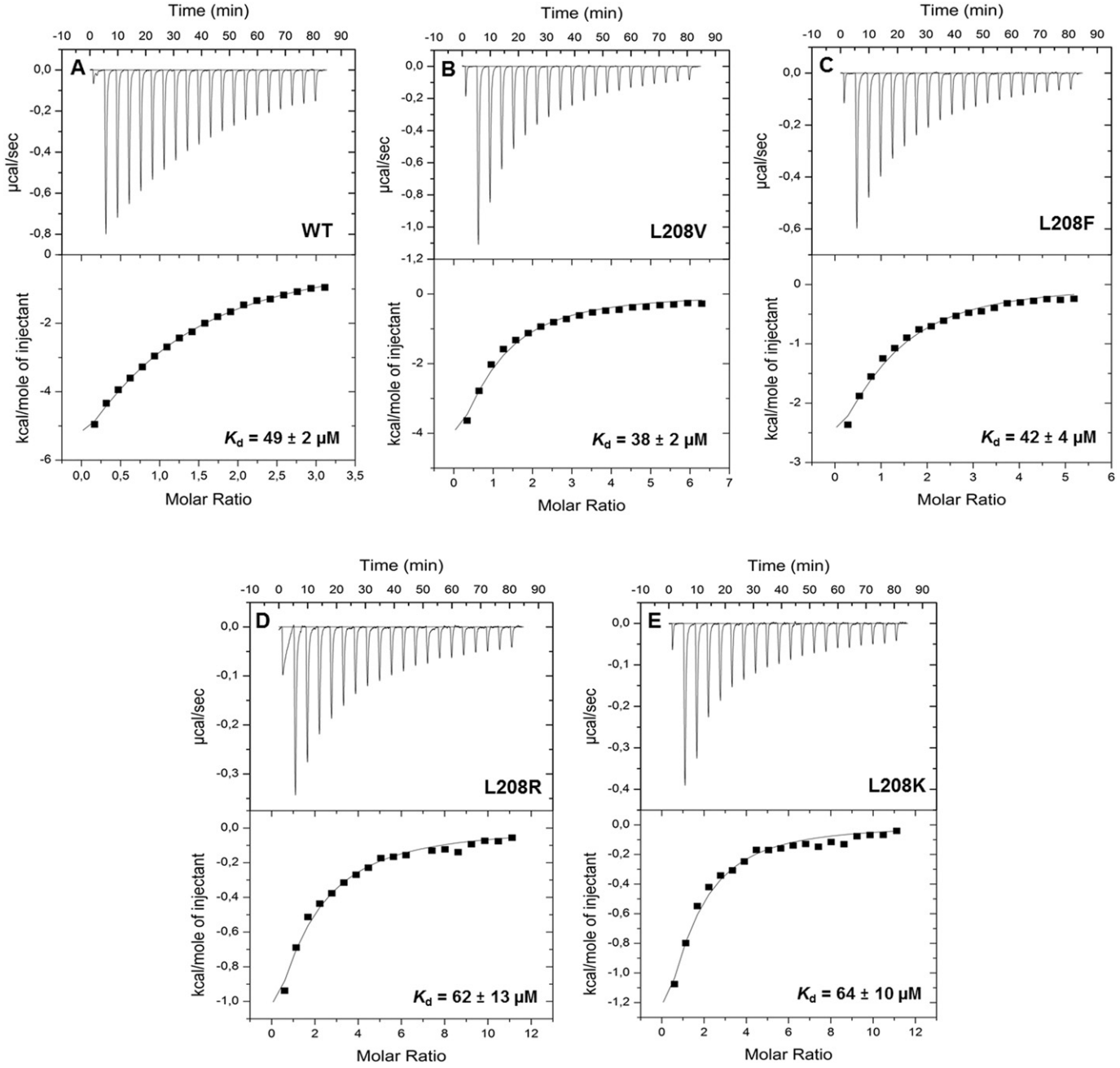

Fig. 3. Binding of SAM to HNMT (wild-type) and L208 variants. ITC experiments were performed in 50 mM Tris-HCl buffer, pH 8.0, containing 100 mM NaCl at 25 °C using a VP-ITC system (MicroCal). Isothermal calorimetric titrations of HNMT (wild-type) (A) and L208 variants for L208V (B), L208F (C), L208R (D) and L208K (E) with SAM are shown. The dissociation constants for SAM binding to HNMT are indicated in panels A-E (see also Table 2).

were conducted as previously described [44,45]. The individual protein bands on a polyacrylamide gel were excised and transferred to a 1.5 mL Eppendorf tube. Each excised gel piece was washed with deionized water prior to be vortexed in 10% acetic acid solution for 10 min. The gel piece was consequently washed with deionized water followed by acetonitrile and a final washing step with deionized water. The stained color of Coomassie Brilliant Blue R250 on each gel piece was removed completely by incubating the gel in a destaining solution containing formic acid:deionized water:isopropanol (1:3:2 *v*/v/v) for 30 min. The gel piece was rinsed with deionized water and dehydrated with acetronitrile. After the destaining procedure, cysteines in the gel piece were alkylated and reduced by iodoacetamide and dithiothreitol (DTT), respectively. Trypsin was then added to digest the protein in the gel at 37 °C overnight. After trypsin digestion, peptide mixtures were extracted and then desalted using ZipTip (Millipore, Darmstadt, Germany). The desalted peptides were spotted onto a MALDI plate with a matrix containing α-cyano-4-hydroxycinnamic acid. The mass spectra of peptides were recorded using a Micromass Tof Spec 2E MALDI-TOF mass spectrometer (Micromass, Cary, NC, USA) in reflectron mode at an accelerating voltage of +20 kV. The instrument was calibrated with a poly(ethylene glycol) mixture (Sigma-Aldrich, St. Louis, MO, USA). ProteoMass™ ACTH Fragments 18–39 (Sigma-Aldrich, St Louis, MO, USA) was used as the peptide calibration standard for the instrument. To analyze mass spectra from the measurement, MassLynx 4.1 (Waters, Milford, MA, USA) was utilized to assign peptide mass profiles.

2.10. In silico prediction of protein stability of the L208 variants

SNPeffect (version 4.0) (http://snpeffect.switchlab.org) [46,47] is a web tool program, which is used to analyze the structural effect of protein variations using various algorithms (TANGO, WALTZ, LIMBO, and FoldX). Protein stability analysis and predicted protein structure for L208 variants were determined and modelled by FoldX. The models for L208 variants were created based on the HNMT wild-type crystal structure (PDB: 1JQD, [29]). The calculation of the free-energy change (ΔΔG) upon variations in the structural phenotype of the protein using FoldX provides information of protein stability of the L208 variants. In addition, the web tool CUPSAT was utilized to analyze and predict protein stability upon substitution of L208 for other amino acids [48].

2.11. Molecular dynamics (MD) simulations of HNMT

The crystal structure of the T105 polymorphic variant of HNMT in complex with *S*-adenosylhomocysteine (SAH) and histamine (PDB:1JQD, chain B) [29] was used as a starting structure for molecular dynamic (MD) simulations (This structure represents an enzyme-substrate complex at pH 5.6, where the enzyme is inactive. An analogous structure at higher pH, where the enzyme is active, was not available in the PDB database). For calculations of HNMT in complex with the methylating cofactor SAM and histamine, which represents the catalytically competent enzymatic complex, a model was created based on the crystal structure. Therefore, a methyl group was tethered to the sulfur atom to give a chiral sulfur center in (S) configuration, which constitutes the biologically active form of SAM [49]. Variants of HNMT were produced by *in silico* point mutations of the created HNMT model. MD simulations and analyses were performed using the YASARA Structure suite, version 13.9.8 (YASARA Biosciences) [50]. A periodic simulation cell that enveloped the whole enzyme with an additional 5 Å margin in each dimension, was used with explicit solvent. The AMBER03 force field [51] was applied and long-range electrostatic potentials were calculated using the Particle Mesh Ewald (PME) method and a cutoff of 7.864 Å [52,53]. The AutoSMILES utility was used to attribute force field parameters to SAH and histamine [54]. For SAM Mulliken charges were generated by single point DFT calculations *via* GAMESS [55], using the B3LYP/6-311G** basis set.

Hydrogen bonding network optimizations were carried out using the method of Hooft and co-workers [56], and pK_a values at pH 7.5 were assigned [57]. The simulation cell was filled with water containing 0.9% of NaCl and a density of 0.993 g/mL. Solvent was relaxed and the system was subsequently energy minimized using steepest descent minimization to remove conformational stress, followed by a simulated annealing minimization step to convergence (<0.05 kJ/mol per 200 steps). Integration time steps were 1.33 and 4 fs for intra- and intermolecular forces, respectively. Subsequently, MD simulations at 310 K were performed,

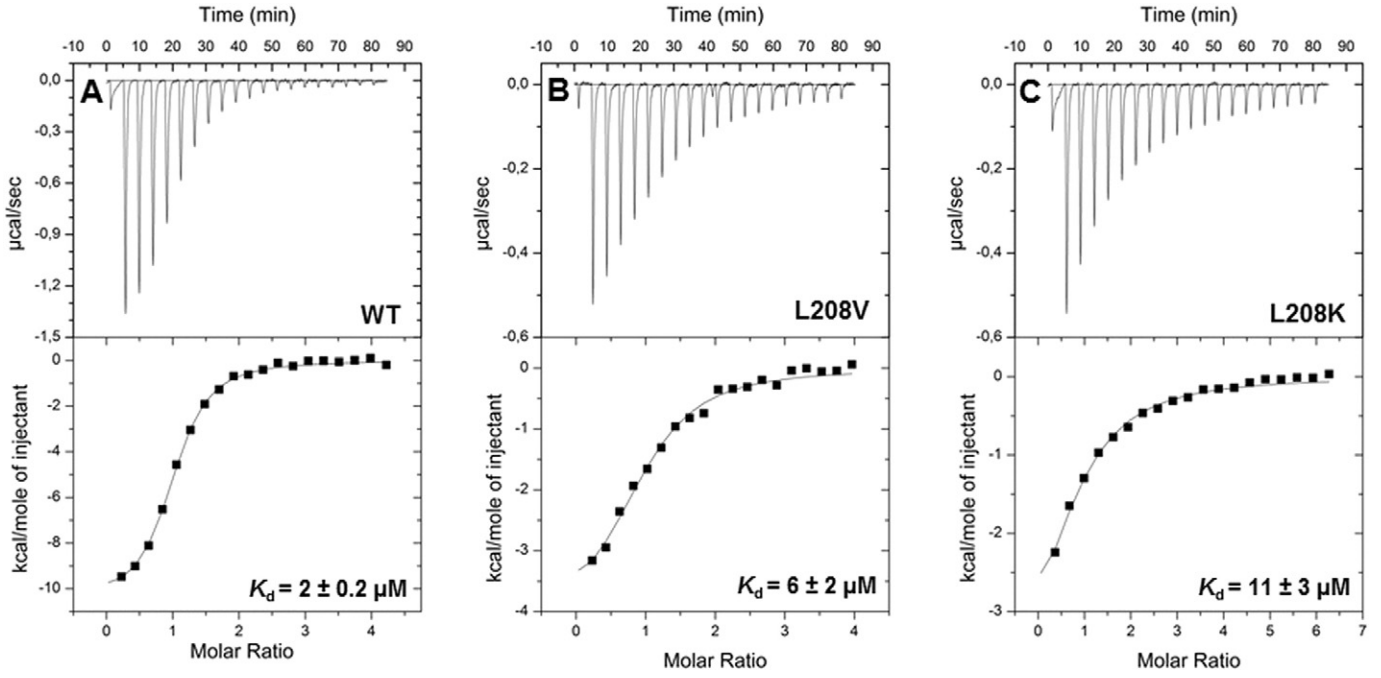

Fig. 4. Binding of SAH to HNMT (wild-type) and L208 variants. ITC experiments were performed in 50 mM Tris-HCl buffer pH 8.0, containing 100 mM NaCl at 25 °C using a VP-ITC system (MicroCal). Isothermal calorimetric titrations of HNMT (wild-type) (A) and L208 variants for L208V (B), and L208K (C) with SAH were presented. The dissociation constants for SAM binding to HNMT (wild-type), L208V, and L208K are indicated in panels A-C (see also Table 2).

Table 2
Dissociation constants (K_d) of HNMT (wild-type) and L208 variants for SAM, SAH and histamine in the presence of SAH by ITC.

HNMT	Dissociation constants (K_d, μM)[a]		
	SAM	SAH	Histamine (in the presence of SAH)
Wild-type	49 ± 2	2 ± 0.2	19 ± 3
L208V	38 ± 2	6 ± 2	ND
L208F	42 ± 4	–	–
L208R	62 ± 13	–	–
L208K	64 ± 10	11 ± 3	ND

ND = not detectable and dash (−) = not measured.
[a] Three independent ITC measurements were conducted for each L208 variant and ligand.

whereby integration time steps for intramolecular and intermolecular forces of 1.25 fs and 2.5 fs were applied, respectively. All MD simulations were carried out in quadruplicate with varying seed numbers and over a time span of 25 ns.

3. Results

3.1. In silico prediction of protein stability

The three-dimensional structure of HNMT shows that the L208 residue is located in one of six helices, termed helix E, flanking a seven-stranded β-sheet of the MTase domain [29]. Although this position is not in or near the active site of HNMT a multiple alignment with vertebrate HNMTs (44–99% identity) revealed that L208 is invariant indicating a conserved structural role of the residue (Fig. 1A and C). In fact L208 has several contacts in the same and the neighboring α-helix as well as the adjacent β-sheet (Fig. 1, panels A and B). Recently, we have reported that *in silico* modeling revealed the drastic destabilizing effect (*ca.* 8 kcal/mol) of the disease-related L208P variant on its structural stability [38]. We concluded that this instability, which correlates with the failure of the enzyme to be expressed as a soluble protein, results in the pathology of the L208P variant. In this context we would like to emphasize that it is difficult to distinguish whether an amino acid replacement blocks folding into the native topology or destabilizes the native topology to such an extent that unfolding is favored. In any case both scenario lead to the depopulation of the folded state of a protein and as a consequence compromise its biological function.

In order to assess further the importance of residue 208 for protein stability we have extended our previous calculations using FoldX in SNPeffect 4.0 [46,47]. As shown in Fig. 1D, all amino acid replacements result in lower protein stability with the strongest effects found for charged amino acids (Arg, Asp, Lys) whereas hydrophobic residues were predicted to exert only a moderate effect on protein stability (1–3 kcal/mol for L208F and L208 V). Results from calculations with FoldX in SNPeffect 4.0 were consistent with protein stability changes predicted by the web tool CUPSAT (data not shown). The analyses confirm that side chain packing in this hydrophobic pocket is critical for the protein's structural stability. This insight prompted us to further investigate protein stability and enzyme activity for the series of HNMT variants displayed in Fig. 1D.

3.2. Protein production and purification of L208 variants

Based on our *in silico* analysis for prediction of protein stability (Fig. 1D) eight variations of human HNMT, *i.e.* L208V, L208F, L208T, L208N, L208R, L208K, L208H, and L208D that covered the whole experimental space in terms of predicted stability and amino acid properties were chosen to be expressed in *E.coli* BL21 (DE3) cells as described in Materials & Methods. The two variants with conservative amino acid exchanges, *i.e.* L208V and L208F were expressed as soluble proteins. In contrast, the variants L208T, L208N, L208H, and L208D were found exclusively in inclusion bodies. Attempts to solubilize these variants by coproduction with chaperones were not successful. Interestingly, the two variants bearing a positively charged amino acid, *i.e.* L208R and L208K, were also detectable as soluble proteins although the stability prediction by FoldX has indicated a profound destabilizing effect

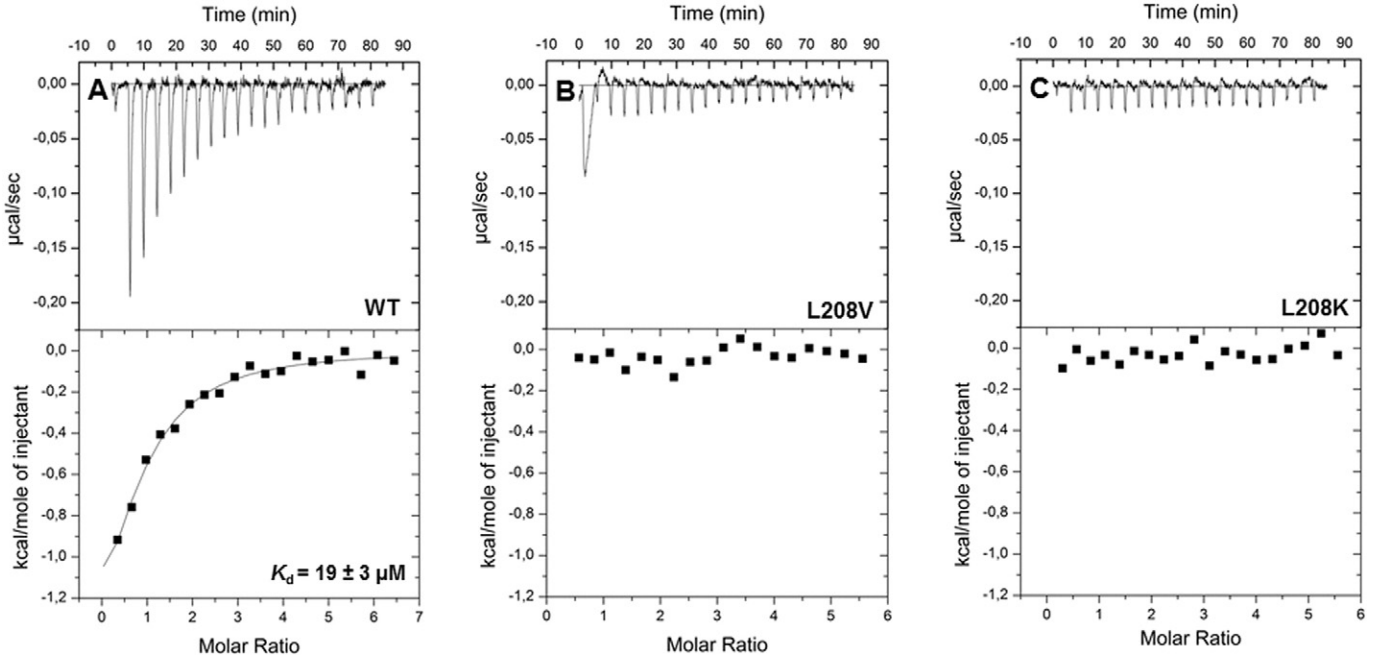

Fig. 5. Binding of histamine to HNMT (wild-type) and L208 variants in the presence of SAH. Isothermal calorimetric titrations of HNMT (wild-type) (A), L208V (B), and L208K (C) variants with histamine in the presence of SAH were performed in 50 mM Tris-HCl buffer pH 8, containing 100 mM NaCl at 25 °C using a VP-ITC system (MicroCal). The ITC experiment for HNMT (wild-type) consisted of 20 consecutive injections of histamine (0.58 mM, 15 μL/injection) into the cell containing 20 μM HNMT (wild-type) and 0.12 mM SAH. For L208V and L208K, a solution of the L208 variants and 0.25 mM SAH in the cell was titrated with histamine (0.50 mM, 15 μL/injection, 20 injections). Data analysis by non-linear least-squares fitting using Origin version 7.0 (Microcal) was conducted to obtain the dissociation constant for histamine binding to HNMT (wild-type) in the presence of SAH. There was no released heat observed after 20 consecutive injections of histamine into the L208 variants in the presence of SAH.

(Fig. 1D). The protein variants expressed in the soluble fraction were purified using a two-step protocol employing Ni-Sepharose affinity and size-exclusion chromatography (see Materials & Methods) as presented in Fig. 2. The yield of purified wild-type protein was 6 mg/g of cell paste. A slightly lower yield of 2 mg/g wet cell paste was achieved with the variants L208V and L208F whereas the yield for the variants L208R and L208K were significantly lower amounting to only 0.2–0.4 mg/g cell paste, respectively (Table 1).

3.3. Determination of dissociation constants using isothermal titration calorimetry (ITC)

We have employed isothermal titration calorimetry (ITC) to determine the affinity of SAM to wild-type HNMT and the soluble variants L208V, L208F, L208R, and L208K. As shown in Fig. 3 (panels A–E), titration of the proteins with SAM at 25 °C produced exothermic signals.

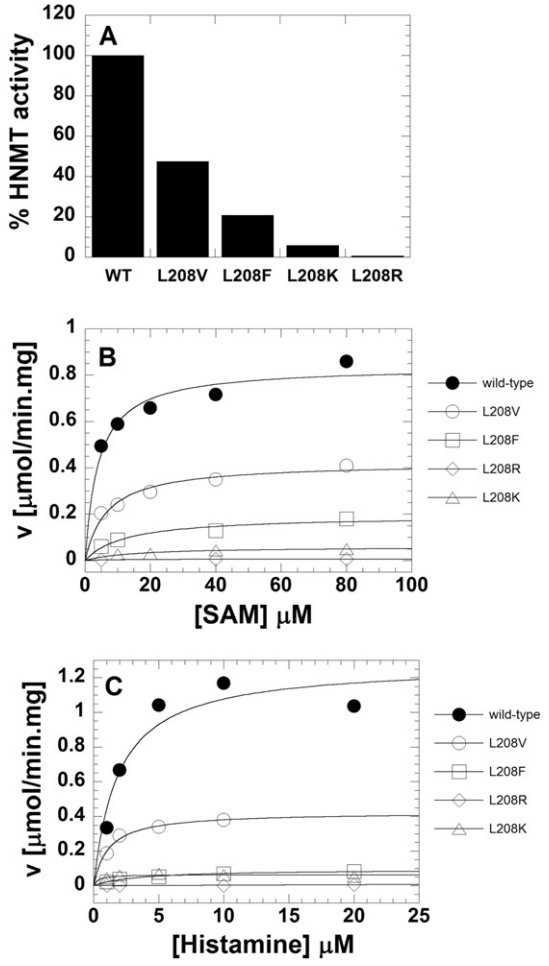

Fig. 6. Catalytic activity and steady-state kinetics of HNMT (wild-type) and L208 variants. (A) Percentage of enzymatic activity of HNMT (wild-type) and L208 variants. (B) Michaelis-Menten plot for HNMT (wild-type) and L208 variant reactions when SAM concentration was varied. Determination of HNMT activity using a radioactive methylation assay was conducted at 25 °C, monitoring the product, methyl-histamine [methyl-, ^{3}H] formation. The reaction contained 20 nM HNMT (wild-type; filled circle, L208V; empty circle, L208F; empty square, L208R; empty diamond, and L208K; empty triangle) in 125 mM bicine buffer pH 8 with 0.15 μCi SAM [methyl-, ^{3}H], 0.025% bovine serum albumin, 1 mM EDTA, a fixed concentration of histamine (40 μM), and various concentrations of SAM (5, 10, 20, 40 and 80 μM). (C) Michaelis–Menten plot for HNMT (wild-type) and L208 variant reactions when the histamine concentration was varied. The HNMT activity was monitored at 25 °C from the reactions consisting of 20 nM HNMT (wild-type; filled circle, L208V; empty circle, L208F; empty square, L208R; empty diamond, and L208K; empty triangle) in 125 mM bicine buffer pH 8, 0.15 μCi SAM [methyl-, ^{3}H], 0.025% bovine serum albumin, 1 mM EDTA, a fixed concentration of SAM (40 μM), and various concentrations of histamine (1, 2, 5, 10 and 20 μM).

The ITC titration data were fitted to a single-binding-site model yielding dissociation constants of 49 ± 2, 38 ± 2, 42 ± 4, 62 ± 13, and 64 ± 10 μM for the wild-type, L208V, L208F, L208R, and L208K, respectively. The results indicate that affinity of SAM to HNMT (wild-type) and the L208 variants is not significantly affected by the amino acid substitution at position 208. Interestingly, the product SAH, binds twenty times more tightly to the wild-type and six times more tightly to the variants L208V and L208K than SAM, exhibiting dissociation constants of 2 ± 0.2, 6 ± 2, and 11 ± 3 μM, respectively (Fig. 4 and Table 2).

In contrast to SAM and SAH, the binding of histamine to HNMT is not detectable by ITC. However, in the presence of SAH, exothermal signals were obtained upon titration with histamine enabling the determination of the dissociation constant by fitting the data to a single-binding-site model. This yielded a dissociation constant of 19 ± 3 μM (Fig. 5, panel A). In the case of the L208V and L208K variants no signals were obtained indicating that histamine binding is substantially affected even in the conservative L208V variant (Fig. 5, panels B and C). A summary of the data obtained by ITC is given in Table 2.

3.4. Catalytic activity of wild-type HNMT and the soluble L208 variants

To determine the effect of amino acid substitutions at position 208 on the catalytic activity, we employed a radioactive methylation assay as described in Materials & Methods [29,40,41]. As shown in Fig. 6 (panel A), product formation (*N*-methylhistamine) was reduced to 48 ± 5%, 21 ± 2%, 6 ± 0.5% and 1 ± 0.05% for the L208V, L208F, L208K and L208R variants, respectively, in comparison to the wild-type enzyme. To gain further insight, a set of steady-state experiments was performed at various concentrations of SAM and histamine. Kinetic parameters of the methylation reaction were obtained by determining the rate of [methyl-^{3}H]-histamine generation as a function of SAM or histamine concentrations (Fig. 6 B and C, respectively) and fitting of the data to the Michaelis-Menten equation. A summary of the kinetic parameters is shown in Table 3. In the case of the L208V variant kinetic parameters are only marginally affected with both K_M values in a similar range as observed for the wild-type and a 3-times lower k_{cat}. The L208F variant is clearly more affected exhibiting significantly higher K_M values and a 5.5-times lower k_{cat}. This tendency is even more pronounced with the L208R and L208K variants. In the case of the former variant no data were obtained due to the low overall activity (see also Fig. 6, panel A).

3.5. Thermal stability of L208 variants of HNMT in the absence and presence of SAM and histamine

The determination of thermal protein stability was performed by a fluorescence-based thermal shift assay (Thermofluor® technique) to obtain the melting temperatures (T_m) of wild-type and the soluble variants (L208V, L208F, L208R, and L208K). This analysis was also carried out in the presence of either SAM or histamine. A compilation of the data is given in Table 4. In the case of the conservative replacements, *i.e.* the L208V and L208F variants, only a slight decrease of the melting temperature was observed. In contrast, the L208R and L208K variants

Table 3
Apparent kinetic parameters of HNMT reaction for HNMT (wild-type) and L208 variants.

HNMT	K_m^{SAM} (μM)	$K_m^{histamine}$ (μM)	k_{cat} (s^{-1})
Wild-type	4.1 ± 1.2	1.9 ± 0.7	0.61 ± 0.08
L208V	6.8 ± 1.6	1.1 ± 0.2	0.23 ± 0.01
L208F	12.4 ± 4.8	3.4 ± 0.5	0.11 ± 0.01
L208R	ND	ND	ND
L208 K	15.0 ± 5.8	ND	0.03 ± 0.006

ND = not detectable.
Enzymatic activity of HNMT was measured using radioactive methylation assay to determine the product formation of methyl-histamine [methyl-, ^{3}H]. Two independent methylation reactions were carried out for each L208 variant an substrate concentration ($p < 0.001$, using a one-way ANOVA).

Table 4
Melting temperature (T_m, °C) of HNMT (wild-type) and L208 variants in the absence and presence of SAM and histamine.

Substrate	Melting temperature (°C)				
	Wild-type	L208V	L208F	L208R	L208 K
No substrate	61.3 ± 2.0*	57.8 ± 2.1*	60.4 ± 2.9^{NS}	48.4 ± 0.6*	53.7 ± 1.8*
+SAM	61.5 ± 0.2*	58.9 ± 0.5*	59.4 ± 1.9*	51.7 ± 0.4*	53.4 ± 0.9*
+Histamine	60.4 ± 2.8*	56.9 ± 1.3*	59.8 ± 2.7 ^{NS}	48.3 ± 0.3*	51.5 ± 2.5*

At least six independent measurements were carried out for each l208 variant in the absence and presence of the substrates. The statistical significance was calculated using one-way ANOVA (* = $p < 0.001$; NS = not significant, *i.e.* $p = 0.169$ and 0.113 for the L208F variant in the absence and presence of histamine, respectively).

showed significantly lower melting temperatures amounting to 13 and 8 °C, respectively. In the presence of either SAM or histamine no significant effects on the melting temperature were observed except for a small thermal stabilization of the L208R variant in the presence of SAM (Table 4). In summary, these results confirm that position 208 plays an important role in maintaining the structural integrity of the protein.

3.6. Determination of the secondary structure of L208 variants of HNMT

To determine the effect of amino acid substitutions on the secondary structure and folding properties, circular dichroism spectra of HNMT (wild-type) and the L208 variants (Supplemental Fig. S1) were recorded. Analysis of the CD spectrum of the wild-type protein using the web tool DichroWeb [42,43] gave a secondary structure composition, as presented in Table 5, which reasonably corresponded to data obtained from the *in-silico* analysis of the crystal structure and showed even better congruence, when compared to the average secondary structure composition predicted from 25 ns MD simulations of HNMT (*vide infra*) using the DSC method in the YASARA suite [58]. In addition, when L208 variants were subjected to the analogous *in silico* analysis, no significant difference in the content of secondary structure compared to the wild-type was observed (Table 5).

3.7. Molecular dynamics (MD) simulations of HNMT

Using the crystal structure of HNMT in complex with SAH and histamine as a starting point, 25 ns MD calculations were performed. The structures showed over all stability over the observed time frame. Generally, a displacement of the histamine ligand was observed. In three of four simulations the histamine was pushed closer to the SAH cofactor, with the deprotonated $N_{\varepsilon 2}$ pointing towards the sulfur atom of SAH (Supplemental Fig. S2) and thus in a suitable orientation and distance for transfer of a methyl group. In one simulation the histamine dissociated from the binding pocket. Analysis of this set of simulations revealed that during all four simulations direct hydrogen bonding of the histamine ligand to amino acid residues, which was observed in the crystal structure, was lost in lieu of hydrogen bonds to surrounding water molecules. Specifically, the intercalation of water molecules between N283, E28 and the aliphatic nitrogen of histamine brought the $N_{\varepsilon 2}$ of histamine closer towards the SAH sulfur (Supplemental Fig. S3). A possible explanation for the repositioning in the MD simulations, as compared to the crystal structure lies in the distinct pH values: While the crystals were obtained at pH 5.6, at which the protein is barely active, MD simulations were performed at pH 7.5, where HNMT shows maximum activity [29]. It is noteworthy that in addition to the structure obtained at pH 5.6, a SeMet structure at pH 7.5 was reported with clearly distinct positioning of the histidine in the active site. Because this structure was not deposited in the PDB database direct comparison to our results was not possible. However, it is clear that the major repositioning of histamine compared to the structure obtained at pH 5.6, as observed in the SeMet counterpart, was not observed as a stable and recurrent conformations in our simulations.

When simulations were repeated for the catalytically competent complex of HNMT, SAM and histamine, the analogous repositioning and 'anchoring' of histamine by water molecules bridging N283 and histamine was observed in all four simulations (Fig. 7, panel A). The positioning of the transfer-methyl group of SAM and the histamine's acceptor atom $N_{\varepsilon 2}$, as seen in trajectory analyses (Fig. 7, panel B), with distances down to ~3.2 Å approximating the van der Waals contact distance, suggests that the MD simulation depicts the catalytically competent enzyme complex. Furthermore, our results suggest that the positioning of histamine in the SAM coordinated HNMT is similar as in the SAH bound complex.

In order to gain insights into the impact of amino acid variations at position 208, 25 ns MD simulations of the respective variants of this study in complex with SAH and histamine were conducted. Substitutions of L208 by V, F, R and K as well as the disease related L208P variant [38] were subjected to MD analysis. The L208P variant, although apparently not stable, was included in our analysis as a reference point, as it contains an effectively helix breaking amino acid. During the 25 ns time period of simulation all investigated structures were stable with similar overall secondary structure content. Inspection of the average structures revealed the presence of two principle conformations, namely an open and closed conformation: the crystal structure, which was also the principle starting structure of all simulations, showed a rather narrow cleft between the helix spanning residues 10–25 and the helix constituted by residues 91–105. In several simulations the distance between these two helices widened considerably (Supplemental Fig. S4). This is consistent with previous findings that dynamic conformational changes from closed to open forms occur in apo-HNMT [31]. Here, as a measure of the conformational state (open *versus* closed), average distances of the Cα of H12 and of Cα of S91 were compiled for all MD simulations (Supplemental Table S2).

While the overall secondary structure content of the structures was not significantly impacted by the investigated amino acid substitutions (Table 5), a significant decrease of the average helical character of helix E was found (Supplemental Table S3), suggesting destabilization of this secondary structure. This effect was also reflected in a local increase in the α-helix's RMSD values (Supplemental Table S2). Notably, the observed effects, a decrease in α-helical secondary structure and increased RMSD values, correlated with the enzyme's activity *in vitro* (Table 3 and Fig. 6), with the strongest impact on the L208R and L208P variants. The destabilization was, however not significantly propagated to other secondary structure elements.

Table 5
Secondary structure content of HNMT (wild-type) and L208 variants.

Secondary-structure content	Wild-type (CD)[c]	Wild-type (PDB)[a]	Wild-type[b]	L208 V[b]	L208F[b]	L208R[b]	L208K[b]	L208P[b]
Helix	38	46	40 ± 1	42 ± 1	42 ± 3	43 ± 3	41 ± 2	42 ± 1
Sheet	17	26	22 ± 1	24 ± 0.5	23 ± 1	24 ± 1	23 ± 1	23 ± 1
Turn	19	10	15 ± 1	13 ± 2	12 ± 3	13 ± 1	15 ± 2	13 ± 1
Coil	27	17	22 ± 2	19 ± 1	21 ± 2	19 ± 2	20 ± 2	22 ± 1
3–10 helix		1	1 ± 1	2 ± 1	2 ± 2	1 ± 1	1 ± 1	1 ± 1

[a] The secondary structure content from the HNMT crystal structure (pdb: 1JQD:chain B).
[b] The average secondary structure content calculated from quadruplicate 25 ns MD simulations using the YASARA suite.
[c] The secondary structure content of HNMT (wild-type) from the CD measurement was analyzed using the Spectra Manager program and the web tool DichroWeb [42,43].

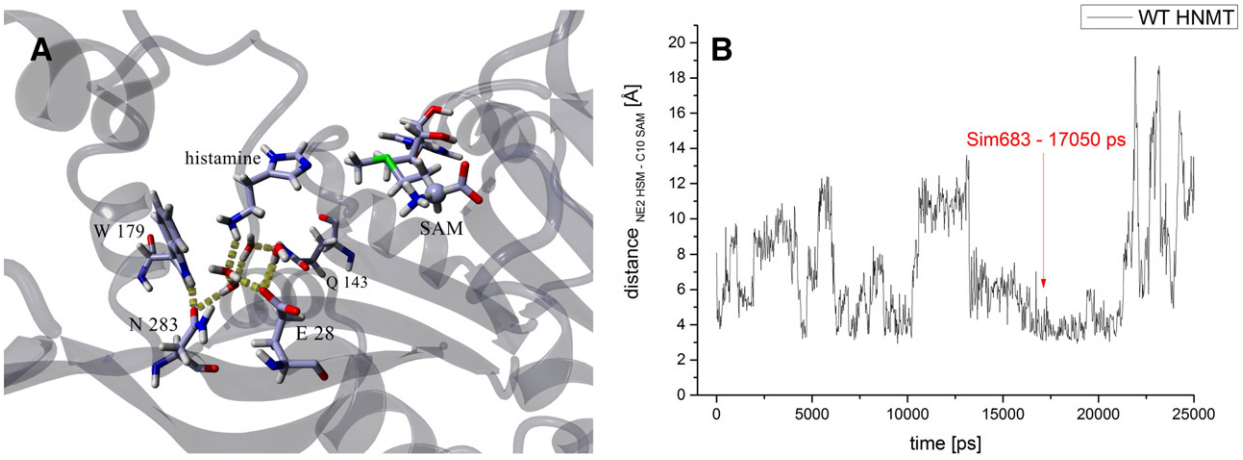

Fig. 7. (A) Active site of HNMT in complex with SAM and histamine showing the hydrogen bonding network (yellow), connecting the aliphatic N of histamine with the protein structure. The 17,050 ps snapshot (snapshot #683) from one MD simulation of the HNMT:SAH:histamine complex at pH 7.5 and 310 K is shown. Nitrogen, oxygen, hydrogen and sulfur atoms are shown in blue, red, white and green, respectively. (B) Trajectory showing the distance of the sulfur bound methyl group of SAM and the recipient atom $N_{\varepsilon 2}$ of histamine. The point of time at which the snapshot from (A) was taken is indicated by a red arrow.

The average histamine's positioning was dramatically disturbed in the variant L208P with the histamine methylation target site $N_{\varepsilon 2}$ ($N_{\varepsilon 2his}$) more remote from the SAH sulfur than the nitrogen of the substrate's aliphatic amino group N_{his} (Table S3). In contrast, in the wild-type the nitrogen of the aliphatic amino group remained at a similar distance and positioning compared to the SAH sulfur in all four simulations, whereas the reorientation of the imidazole ring away from the SAH, resulting in a greater distance of $N_{\varepsilon 2}$ to the sulfur only occurred in one instance. The variant L208F showed a similar behavior as the variant L208P with the histamine consistently reoriented and at greater distances than in the wild-type. In the variants L208R and L208K deviations from average position of the histamine in the wild-type are still observable but less pronounced. Surprisingly, the histamine appears to be drawn closer to SAH in the L208K variant than in other structures. The data are summarized in Supplemental Table S2 and average data for all four simulations are given in Table 6. Average distances and standard deviations for a set of four MD simulations show that S_{SAH} - N_{his} distances are strongly conserved in the wild-type, while distances and their variations fluctuate in the variants, indicating that the 'anchoring' of histamine *via* its aliphatic nitrogen atom is disturbed. This was further confirmed by the visual inspection of average protein structures.

In order to assess how amino acid replacements at position 208 alter the binding site of histamine structures obtained in our MD simulations were analyzed in more detail. In this context, it is noteworthy that no correlation between the open and closed conformation of HNMT and the positioning of histamine was observed. Visual inspection of the protein crystal structure as well as average structures from MD simulations showed that S201 in α-helix E forms a hydrogen bond to S286 in the adjacent β-strand, which is separated by only two amino acids from N283, the residue apparently responsible for the correct anchoring of the nitrogen atom of the aliphatic amino group (Fig. 8). A relative destabilization and greater mobility of the α-helix in the variants, as observed in our simulations (Supplemental Table S2 and S3), may propagate to N283 and thus compromise histamine binding. This in turn could reasonably rationalize the observed impaired catalytic activity of the variants that correlates with the increase in α-helix destabilization. Equally, introduction of large amino acids in position 208, *e.g.* phenylalanine and arginine, leads to clashes with Y215 (Fig. 8), which is located in the same adjacent β-strand as S286, and may thus disturb the positioning of histamine by N283 in a similar fashion.

Table 6
Average distances of $N_{\varepsilon 2}$ and aliphatic N of histamine to the sulfur of SAH (S_{SAH}) and their variance, determined from a set of four MD simulations.

	S_{SAH}-$N_{\varepsilon 2his}$		S_{SAH}-N_{his}	
	Average distance [Å] ($N = 4$)	STDEV ($N = 4$)	Average distance [Å] ($N = 4$)	STDEV ($N = 4$)
Wild-Type	8.2	2.1	9.1	0.2
L208V	8.3	1.9	10	0.2
L208F	11.4	2.2	10	1.4
L208R	8.9	2.4	10.7	1.4
L208K	7.9	3	8.7	0.8
L208P	11.5	2.6	10	1

4. Discussion

The L208P variant of human HNMT was recently discovered as the cause of intellectual disability although inspection of the crystal structure did not provide a clear rationale for the putative dysfunction of the enzyme in histamine degradation. Analysis of the impact of the replacement of leucine by other amino acids with either charged (R, K, H and D), polar (T, N) or apolar (V, F) side chains suggested a clear relationship disfavoring charged and polar residues in comparison to apolar residues (Fig. 1D). This concept was borne out for the majority of variants bearing charged or polar side chains with the notable exception of the L208 K and L208R variants. These variants could be isolated and partially characterized although they were predicted to be less stable than the L208T, L208H or L208N variants. This unforeseen stability of the L208K and L208R variant could be due to the length of the side chain that places the positively charged amino or guanidine group closer to the surface and thus alleviates the unfavorable contacts to the hydrophobic amino acid side chains in the vicinity of position 208.

The four variants L208V, L208F, L208K and L208R were isolated in varying amounts. Whereas the yields for the L208V and L208F variants were only reduced three-fold the latter two variants showed a thirty-fold decrease (Table 1). This apparent difference in stability was also reflected by the melting temperatures, which were slightly lower for the L208F and L208V but much more severely reduced for the L208K and L208R variants (Table 4). A similar tendency was observed in steady-state measurements that showed slightly reduced enzymatic activity for the L208V and L208F variants while the L208K and L208R variants exhibited <5% residual activity (Fig. 6 and Table 3). This initial characterization of the generated variants clearly suggested that position 208 is very sensitive to amino acid replacements resulting in a deterioration of stability and enzyme function, which strongly depends on the properties of the amino acid side chain.

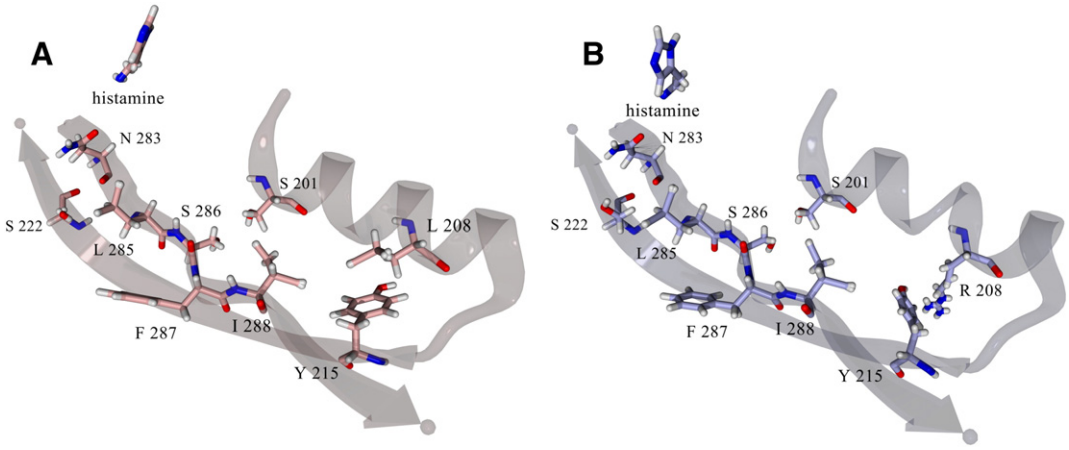

Fig. 8. Cartoon showing the structural features that link the residue 208 bearing α-helix, which spans residues 200–212, with residues lining the histamine binding pocket in HNMT. Average structures from 25 ns simulations of (A) wild-type HNMT and (B) the L208R variant are shown. The histamine ligand and selected amino acids, which link the respective secondary structures through side chain interactions are shown. Hydrogen, nitrogen and oxygen atoms are shown in white, blue and red, respectively. Carbon atoms are shown in pink (A) and grey (B).

In order to obtain further insights into the molecular mechanism by which the amino acid in position 208 exerts its influence on enzymatic activity we investigated the binding of SAM, SAH and histamine to the variants. Interestingly, binding of SAM and SAH was apparently not much affected in any of the variants with only a moderately higher dissociation constant for SAM and SAH for the L208K and L208R variants (Figs. 3 and 4; Table 2). In contrast, histamine binding as demonstrated by ITC measurements (in the presence of SAH) was only detectable for wild-type protein and even the L208V variant appeared to be compromised in histamine binding (Fig. 5). This result suggests that the effect on histamine binding is the major cause for the deterioration of enzymatic function in the variants. However, it was still not clear how amino acid exchanges in position 208 affect the binding of histamine. To address this question, we have carried out molecular dynamics (MD) calculations on the basis of the previously reported crystal structure of the HNMT:SAH:histamine complex ([29], PDB: 1JQD).

In our MD simulations we have noticed that histamine repositions in the active site to adopt a suitable position and orientation for the transfer of a methyl group from SAM to the $N_{\varepsilon 2}$, *i.e.* the crystal structure does not reflect a catalytically competent complex. This difference is obviously the consequence of the different pH values used for crystallization and our simulations, respectively. While crystallization was conducted at a low pH where the enzyme is inactive, we have used a physiological pH where the enzyme is active. Thus the observed repositioning of histamine appears to be triggered by the difference in pH used in the MD simulations.

Binding and positioning of histamine appears to be mainly achieved by interactions of the aliphatic amino group with water molecules, which are hydrogen bonding to the side chains of N283 and E28. Although position 208 is remote from the histamine binding pocket our simulations have indicated that amino acid exchanges destabilize the resident α-helix and this in turn disturbs side chain interactions with the adjacent β-strand that contains N283. Thus amino acid replacements in position 208 exert a long-range effect that propagates from α-helix E to the adjacent β-strand and eventually affects amino acids directly involved in histamine binding. This scenario is supported by our observation that the degree of α-helix destabilization and the loss of catalytic activity correlate. The resulting disturbance of histamine binding can potentially impact both histamine affinity (K_d) and the correct positioning of histamine for methylation and, consequently, the rate at which methylation occurs.

This effect from a single amino acid exchange was also observed in another polymorphic SAM-dependent methyl transferase, thiopurine *S*-methyltransferase (TPMT). The amino acid replacement of a tyrosine by a cysteine at position 240 (TPMT*3C, the Y240C variant), which is located in β-strand 9, reduced enzymatic activity [59] and lowered the melting temperature from 50 to 39 °C [60,61]. Although no overall structural differences were observed in the Y240C variant, MD simulations indicated a loss of side chain interactions between β-strand 9 and the adjacent helix α8, which in turn appears to affect the substrate binding site [62]. Another SAM-dependent transferase, catechol *O*-methyltransferase (COMT), exhibits a similar structural alteration in the V108M variant. Again, this position is ~16 Å apart from the SAM-binding site, but the amino acid exchange causes the reorientation of a proximal helix, resulting in the perturbation of the SAM and substrate binding sites [63,64].

Transparency document

The Transparency document associated with this article can be found, in online version.

Acknowledgements

This work was supported by a grant from the Austrian Science Foundation (FWF) (W901) to GS and PM (Doctoral program "Molecular Enzymology" W901) and the Austrian Academic Service (ÖAD) through a Technology Grant Southeast Asia to CT.

Appendix A. Supplementary data

Supplementary data to this article can be found online at http://dx.doi.org/10.1016/j.bbadis.2016.10.005.

References

[1] A. Falus, N. Grosman, Z. Darvas, Histamine: Biology and Medical Aspects, SpringMed Publishing, Budapest, 2004.
[2] L. Rosenwasser, New insights into the pathophysiology of allergic rhinitis, Allergy Asthma Proc. 28 (2007) 10–15.
[3] J. Loiselle, A. Wollin, Mucosal histamine elimination and its effect on acid secretion in rabbit gastric mucosa, Gastroenterology 104 (1993) 1013–1020.
[4] M. Zhang, R.L. Thurmond, P.J. Dunford, The histamine H(4) receptor: a novel modulator of inflammatory and immune disorders, Pharmacol. Ther. 113 (2007) 594–606.
[5] J.C. Schwartz, J.M. Arrang, M. Garbarg, H. Pollard, M. Ruat, Histaminergic transmission in the mammalian brain, Physiol. Rev. 71 (1991) 1–51.
[6] L.B. Hough, Cellular localization and possible functions for brain histamine: recent progress, Prog. Neurobiol. 30 (1988) 469–505.

[7] H. Wada, N. Inagaki, A. Yamatodani, T. Watanabe, Is the histaminergic neuron system a regulatory center for whole-brain activity? Trends Neurosci. 14 (1991) 415–418.
[8] A. Molina-Hernández, N.F. Díaz, J.A. Arias-Montaño, Histamine in brain development, J. Neurochem. 122 (2012) 872–882.
[9] P. Panula, M. Lintunen, K. Karlstedt, Histamine in brain development and tumors, Semin. Cancer Biol. 10 (2000) 11–14.
[10] A. Molina-Hernández, I. Velasco, Histamine induces neural stem cell proliferation and neuronal differentiation by activation of distinct histamine receptors, J. Neurochem. 106 (2008) 706–717.
[11] L. Maintz, N. Novak, Histamine and histamine intolerance, Am. J. Clin. Nutr. 85 (2007) 1185–1196.
[12] P.J. Barnes, Anti-IgE therapy in asthma: rationale and therapeutic potential, Int. Arch. Allergy Immunol. 123 (2000) 196–204.
[13] H. Haas, P. Panula, The role of histamine and the tuberomamillary nucleus in the nervous system, Nat. Rev. Neurosci. 4 (2003) 121–130.
[14] H.L. Haas, O.A. Sergeeva, O. Selbach, Histamine in the nervous system, Physiol. Rev. 88 (2008) 1183–1241.
[15] S.J. Hill, C.R. Ganellin, H. Timmerman, J.C. Schwartz, N.P. Shankley, J.M. Young, W. Schunack, R. Levi, H.L. Haas, International union of pharmacology. XIII. Classification of histamine receptors, Pharmacol. Rev. 49 (1997) 253–278.
[16] I.J. de Esch, R.L. Thurmond, A. Jongejan, R. Leurs, The histamine H4 receptors as a new therapeutic target for inflammation, Trends Pharmacol. Sci. 26 (2005) 462–469.
[17] C. Maslinski, W.A. Fogel, Catabolism of histamine, in: B. Uvnäs (Ed.), Handbook of Experimental Pharmacology, Histamine and Histamine Antagonists, Vol 97, Springer, Berlin- Heidelberg 1991, pp. 165–189.
[18] H.G. Schwelberger, F. Ahrens, W.A. Fogel, F. Sánchez-Jiménez, Chapter 3: histamine metabolism, in: H. Stark (Ed.), Histamine H_4 Receptor: A Novel Drug Target for Immunoregulation and Inflammation, Versita, London 2013, pp. 63–102.
[19] M.A. Beaven, Histamine: its role in physiological and pathological processes, Monogr. Allergy 13 (1978) 1–113.
[20] S. Okinaga, T. Ohrui, H. Nakazawa, K. Yamauchi, E. Sakurai, T. Watanabe, K. Sekizawa, H. Sasaki, The role of HMT (histamine *N*-methyltransferase) in airways: a review, methods find, Exp. Clin. Pharmacol. 17 (Suppl. C) (1995) 16–20.
[21] G.L. Chen, B. Zhu, W.P. Nie, Z.H. Xu, Z.R. Tan, G. Zhou, J. Liu, W. Wang, H.H. Zhou, Single nucleotide polymorphisms and haplotypes of histamine *N*-methyltransferase in patients with gastric ulcer, Inflamm. Res. 53 (2004) 484–488.
[22] W.P. Burkard, K.F. Gey, A. Pletscher, Diamine oxidase in the brain of vertebrates, J. Neurochem. 10 (1963) 183–186.
[23] D.D. Brown, R. Tomchick, J. Axelrod, The distribution and properties of a histamine-methylating enzyme, J. Biol. Chem. 234 (1959) 2948–2950.
[24] K.M. Lindahl, The histamine methylating enzyme system in liver, Acta Physiol. Scand. 49 (1960) 119–138.
[25] C.V. Preuss, T.C. Wood, C.L. Szumlanski, R.B. Raftogianis, D.M. Otterness, B. Girard, M.C. Scott, R.M. Weinshilboum, Human histamine *N*-methyltransferase pharmacogenetics: common genetic polymorphisms that alter activity, Mol. Pharmacol. 53 (1998) 708–717.
[26] B. Girard, D.M. Otterness, T.C. Wood, R. Honchel, E.D. Wieben, R.M. Weinshilboum, Human histamine *N*-methyltransferase pharmacogenetics: cloning and expression of kidney cDNA, Mol. Pharmacol. 45 (1994) 461–468.
[27] K. Yamauchi, K. Sekizawa, H. Suzuki, H. Nakazawa, Y. Ohkawara, D. Katayose, H. Ohtsu, G. Tamura, S. Shibahara, M. Takemura, et al., Structure and function of human histamine *N*-methyltransferase: critical enzyme in histamine metabolism in airway, Am. J. Phys. 267 (1994) L342–L349.
[28] S. Aksoy, R. Raftogianis, R.M. Weinshilboum, Human histamine *N*-methyltransferase gene: structural characterization and chromosomal localization, Biochem. Biophys. Res. Commun. 219 (1996) 548–554.
[29] J.R. Horton, K. Sawada, M. Nishibori, X. Zhang, X. Cheng, Two polymorphic forms of human methyltransferase: structure, thermal, and kinetic comparisons, Structure 9 (2001) 837–849.
[30] J.R. Horton, K. Sawada, M. Nishibori, X. Cheng, Structure basis for inhibition of histamine *N*-methyltransferase by diverse drugs, J. Mol. Biol. 353 (2005) 334–344.
[31] K. Rutherford, W.W. Parson, V. Daggett, The histamine *N*-methyltransferase T105I polymorphism affects active site structure and dynamics, Biochemistry 47 (2008) 893–901.
[32] L. Yan, R.E. Galinsky, J.A. Bernstein, S.B. Liggett, R.M. Weinshilboum, Histamine *N*-methyltransferase pharmacogenetics: association of a common functional polymorphism with asthma, Pharmacogenetics 10 (2000) 261–266.
[33] E. García-Martín, J. García-Menaya, B. Sánchez, C. Martínez, R. Rosendo, J.A.G. Agúndez, Polymorphisms of histamine-metabolizing enzymes and clinical manifestations of asthma and allergic rhinitis, Clin. Exp. Allergy 37 (2007) 1175–1182.
[34] M.C. Ledesma, E. García-Martín, H. Alonso-Navarro, C. Martínez, F.J. Jiménez-Jiménez, J. Benito-León, I. Puertas, L. Rubio, T. López-Alburquerque, J.A.G. Agúndez, The nonsynonymous Thr105Ile polymorphism of the histamine *N*-methyltransferase is associated to the risk of developing essential tremor, Neuromol. Med. 10 (2008) 356–361.
[35] V. Palada, J. Terzić, J. Mazzulli, G. Bwala, J. Hagenah, B. Peterlin, A.Y. Hung, C. Klein, D. Krainc, Histamine *N*-methyltransferase Thr105Ile polymorphism is associated with Parkinson's disease, Neurobiol. Aging 33 (2012) 836.e1–836.e3.
[36] L. Kaufman, M. Ayub, J.B. Vincent, The genetic basic of non-syndromic intellectual disability: a review, J. Neurodevelop. Disord. 2 (2000) 182–209.
[37] P.K. Maulik, M.N. Mascarenhas, C.D. Mathers, T. Dua, S. Saxena, Prevalence of intellectual disability: a meta-analysis of population based studies, Res. Dev. Disabil. 32 (2011) 419–436.
[38] A. Heidari, C. Tongsook, R. Najafipour, L. Musante, N. Vasli, M. Garshasbi, H. Hu, K. Mittal, A.J. McNaughton, K. Sritharan, M. Hudson, H. Stehr, S. Talebi, M. Moradi, H. Darvish, M. Arshad Rafiq, H. Mozhdehipanah, A. Rashidinejad, S. Samiei, M. Ghadami, C. Windpassinger, G. Gillessen-Kaesbach, A. Tzschach, I. Ahmed, A. Mikhailov, D.J. Stavropoulos, M.T. Carter, S. Keshavarz, M. Ayub, H. Najmabadi, X. Liu, H.H. Ropers, P. Macheroux, J.B. Vincent, Mutations in the histamine *N*-methyltransferase gene, HNMT, are associated with nonsyndromic autosomal recessive intellectual disability, Hum. Mol. Genet. 24 (2015) 5697–5710.
[39] S.K. Shapiro, D.J. Ehninger, Methods for the analysis and preparation of adenosylmethionine and adenosylhomocysteine, Anal. Biochem. 15 (1966) 323–333.
[40] K.M. Verburg, R.R. Bowsher, D.P. Henry, A new radioenzymatic assay for histamine using purified histamine *N*-methyltransferase, Life Sci. 32 (1983) 2855–2867.
[41] R.R. Bowsher, K.M. Verburg, D.P. Henry, Rat histamine *N*-methyltransferase. Quantification, tissue distribution, purification, and immunologic properties, J. Biol. Chem. 258 (1983) 12215–12220.
[42] L. Whitmore, B.A. Wallace, Protein secondary structure analyses from circular dichroism spectroscopy: methods and reference databases, Biopolymers 89 (2008) 392–400.
[43] L. Whitmore, B.A. Wallace, DICHROWEB, an online server for protein secondary structure analyses from circular dichroism spectroscopic data, Nucleic Acids Res. 32 (2004) W668–W673.
[44] W.D. Lienhart, V. Gudipati, M.K. Uhl, A. Binter, S.A. Pulido, R. Saf, K. Zangger, K. Gruber, P. Macheroux, Collapse of the native structure caused by a single amino acid exchange in human NAD(P)H:quinone oxidoreductase, FEBS J. 281 (2014) 4691–4704.
[45] R.L. Gundry, M.Y. White, C.I. Murray, L.A. Kane, Q. Fu, B.A. Stanley, J.E. Van Eyk, Preparation of proteins and peptides for mass spectrometry analysis in a bottom-up proteomics workflow, Curr. Protoc. Mol. Biol. Chapter 10 (2009) (Unit10.25).
[46] G. De Baerts, J. Van Durme, J. Reumers, S. Maurer-Stroh, P. Vanhee, J. Dopazo, J. Schymkowitz, F. Rousseau, SNPeffect 4.0: on-line prediction of molecular and structural effects of protein-coding variants, Nucleic Acids Res. 40 (2012) D935–D939.
[47] J. Schymkowitz, J. Borg, F. Stricher, R. Nys, F. Rousseau, L. Serrano, The FoldX web server: an online force field, Nucleic Acids Res. 33 (2005) W382–W388.
[48] V. Parthiban, M.M. Gromiha, D. Schomburg, CUPSAT: prediction of protein stability upon point mutations, Nucleic Acids Res. 34 (Suppl. 2) (2006) W239–W242.
[49] G. de la Haba, G.A. Jamieson, S.H. Mudd, H.H. Richards, S-adenosylmethionine: the relation of configuration at the sulfonium center to enzymatic reactivity, J. Am. Chem. Soc. 81 (1959) 3975–3980.
[50] YASARA (13.9.8), YASARA Biosciences GmbH, Vienna, Austria, 2012.
[51] J. Wang, P. Cieplak, P.A. Kollman, How well does a restrained electrostatic potential (RESP) model perform in calculating conformational energies of organic and biological molecules? J. Comput. Chem. 21 (2000) 1049–1074.
[52] W.D. Cornell, P. Cieplak, C.I. Bayly, I.R. Gould, K.M. Merz Jr., D.M. Ferguson, D.C. Spellmeyer, T. fox, J.W. Caldwell, P.A. Kollman, A second generation force field for the simulation of proteins, nucleic acids, and organic molecules, J. Am. Chem. Soc. 117 (1995) 5179–5197.
[53] U. Essman, L. Perera, M.L. Berkowitz, T. Darden, H. Lee, L.G. Pedersen, A smooth particle mesh Ewald method, J. Chem. Phys. 103 (1995) 8577–8593.
[54] A. Jakalian, D.B. Jack, C.I. Bayly, Fast, efficient generation of high-quality atomic charges. AM1-BCC model: II. Parameterization and validation, Comput. Chem. 23 (2002) 1623–1641.
[55] M.F. Guest, I.J. Bush, H.J.J. van Dam, P. Sherwood, J.M.H. Thomas, J.H. van Lenthe, R.W.A. Havenith, J. Kendrick, The GAMESS-UK electronic structure package: algorithms, developments and applications, Mol. Phys. 103 (2005) 719–747.
[56] R.W. Hooft, G. Vriend, C. Sander, E.E. Abola, Errors in protein structures, Nature 381 (1996) 272.
[57] E. Krieger, J.E. Nielsen, C.A. Spronk, G.J. Vriend, Fast empirical pKa prediction by Ewald summation, Mol. Graph. Model. 25 (2006) 481–486.
[58] R.D. King, M.J. Sternberg, Identification and application of the concepts important for accurate and reliable protein secondary structure and prediction, Protein Sci. 5 (1996) 2298–2310.
[59] H.L. Tai, M.Y. Fessing, E.J. Bonten, Y. Yanishevsky, A. d'Azzo, E.Y. Krynetski, W.E. Evans, Enhanced proteasomal degradation of mutant human thiopurine *S*-methyltransferase (TPMT) in mammalian cells: mechanism for TPMT protein deficiency inherited by TPMT*2, TPMT*3 A, TPMT*3B or TPMT*3C, Pharmacogenetics 9 (1999) 641–650.
[60] L. Wang, T.V. Nguyen, R.W. McLaughlin, L.A. Sikkink, M. Ramirez-Alvarado, R.M. Weinshilboum, Human thiopurine *S*-methyltransferase pharmacogenetics: variant allozyme misfolding and aggresome formation, Proc. Natl. Acad. Sci. U. S. A. 102 (2005) 9394–9399.
[61] H. Wu, J.R. Horton, K. Battaile, A. Allali-Hassani, F. Martin, H. Zeng, P. Loppnau, M. Vedadi, A. Bochkarev, A.N. Plotnikov, X. Cheng, Structural basis of allele variation of human thiopurine-*S*-methyltransferase, Proteins 67 (2007) 198–208.
[62] K. Rutherford, V. Daggett, Four human thiopurine *S*-methyltransferase alleles severely affect protein structure and dynamics, J. Mol. Biol. 379 (2008) 803–814.
[63] K. Rutherford, B.J. Bennion, W.W. Parson, V. Daggett, The 108 M polymorph of human catechol *O*-methyltransferase is prone to deformation at physiological temperatures, Biochemistry 45 (2006) 2178–2188.
[64] K. Rutherford, V. Daggett, Polymorphisms and disease: hotspots of inactivation in methyltransferases, Trends Biochem. Sci. 35 (2010) 531–538.